Detection of periprosthetic fractures around the femoral stem by resonance frequency analysis: An in vitro study

Anne-Sophie Poudrel, Giuseppe Rosi, Vu-Hieu Nguyen, Victor Housset, Charles-Henri Flouzat-Lachaniette, Guillaume Haiat

Detection of periprosthetic fractures around the femoral stem by resonance frequency analysis: an *in vitro* study

Anne-Sophie Poudrel[1], Giuseppe Rosi[2], Vu-Hieu Nguyen[2], Victor Housset[4,5], Charles-Henri Flouzat-Lachaniette[4,5], and Guillaume Haiat[*1]

[1]CNRS, Univ Paris Est Creteil, Univ Gustave Eiffel, UMR 8208, MSME, F-94010 Créteil, France

[2]Univ Paris Est Creteil, Univ Gustave Eiffel, CNRS, UMR 8208, MSME, F-94010 Créteil, France

[4]Service de Chirurgie Orthopédique et Traumatologique, Hôpital Henri Mondor AP-HP, CHU Paris 12, Université Paris-Est, Créteil, France

[5]INSERM U955, IMRB Université Paris-Est, Créteil, France

Abstract

Periprosthetic femoral bone fractures are frequent complications of Total Hip Arthroplasty (THA) and may occur during the insertion of uncemented Femoral Stems (FS), due to the nature of the press-fit fixation. Such fracture may lead to the surgical failure of the THA and require a revision surgery, which may have dramatic consequences. Therefore, an early detection of intra-operative fractures is important to avoid worsening the fracture and/or to enable a peroperative treatment. The aim of this *in vitro* study is to determine the sensitivity of a method based on resonance frequency analysis of the bone-stem-ancillary system for periprosthetic fractures detection. A periprosthetic fracture was artificially created close to the lesser-trochanter of ten femoral bone mimicking phantoms. The bone-stem-ancillary resonance frequencies in the range [2-12] kHz were measured on an ancillary instrumented with piezoelectric sensors, which was fixed to the femoral stem. The measurements were repeated for different fracture lengths from 4 mm to 55 mm. The results show a decrease of the resonance frequencies due to the fracture occurrence and propagation. The frequency shift reached up to 170 Hz. The minimum fracture length that can be detected varies from 3.1 ± 1.7 mm to 5.9 ± 1.9 mm according to the mode and to the specimen. A significantly higher sensitivity ($p=0.011$) was obtained for a resonance frequency around 10.6 kHz, corresponding to a mode vibrating in a plane perpendicular to the fracture. This study opens new paths towards the development of non-invasive vibration-based methods for intra-operative periprosthetic fractures detection.

Keywords femoral stem, periprosthetic fracture, resonance frequency, vibration analysis, non-invasive method

*Corresponding author : guillaume.haiat@cnrs.fr

1 Introduction

Total hip arthroplasty (THA) is a routine surgery which is increasingly performed, mainly due to population aging. In the United States, the number of THAs performed each year is expected to reach more than a million before 2040 (1). Uncemented THAs have become more and more employed by the surgeons in the last few years, reaching up to 80% of the procedures in several countries (2). The initial stability of the uncemented implants is achieved through press-fitting the implant into a host bone cavity, previously reamed by the surgeon, by successive hammer impacts. Due to the nature of the fixation based on implant press-fit, the risk of periprosthetic fractures, which are defined as both intra-operative and post-operative fractures, is one of the most frequent causes of revision. In particular, uncemented femoral stems (FS) (3; 4) have a rate of periprosthetic fracture significantly higher than the cemented ones (5; 6). Moreover, the fracture incidence, prevalent during revision surgeries (7) can reach up to 28% for uncemented THA (8), which makes it one of the most challenging issues for the surgeons related to the insertion of uncemented FS (9).

Due to the nature of the fixation and the shape of the FS implants, the risk of calcar cracks and shaft fractures is significantly increased for uncemented implants (10; 11). A classification of the fracture types based on their location on the femoral bone was proposed by (12) during a recent mid-term follow-up study. In 42% of the cases, the fracture occurs close to the lesser-trochanter, namely the fractures of type I. A numerical study (13) confirms these observations by showing that the region of the femur which is subjected to the highest stresses corresponds to the zone of occurrence of fracture of type I according to the classification of (12). Considering the Vancouver classification of femoral periprosthetic fractures developed by (14) and largely employed nowadays for categorizing the configuration of periprosthetic proximal femoral fractures and for planning their management (15; 16), these fractures correspond to type A and B. While the fractures of type A stay confined to the proximal metaphysis and involve the greater and lesser trochanter, the fractures of type B involve the diaphysis region. The fractures of type B are then subdivided depending on the stability of the implant: the type B1 correspond to a stable implant whereas the types B2 and B3 are associated with a loss of implant stability, depending on the seriousness of implant loosening (17; 16).

Fractures are often not detected during the surgery and are later characterized in postoperative radiographs (18). However, undetected fractures during the surgery may lead to aseptic loosening because of poor osseointegration and of a lack of bone ingrowth (19). Therefore, fractures peroperative detection is an important issue in order to avoid revision surgery. On the one hand, early intra-operative fracture detection allows the surgeon to adapt the insertion procedure in order to avoid the fracture worsening because of the later hammer impacts. On the other hand, the intra-operative diagnosis allows the surgeon to treat the fracture appropriately during the time of surgery by cerclage wires or bone graft for instance (20; 21; 19; 3).

Quantitative methods have widely been studied in the literature for FS insertion monitoring into the host bone. Most of them are based on impact force analysis (22; 23; 24), vibration analysis (25; 26; 27; 28; 29) or acoustics measurements (30; 31; 32; 33). Among these studies aiming at assessing the insertion of the FS, a limited number has been tested to detect periprosthetic fractures. In particular, vibro-acoustic methods

have shown promising results concerning their use for periprosthetic fracture detection (28; 30; 31). In a recent *in vivo* study about the assessment of acoustic analysis to monitor implant seating, Goossens et al. (30) observed a significant change of the bone-implant system acoustic behavior with a fracture occurrence. However, this observation was based only on three intra-operative fractures and no quantitative criterion could be developed. A significant difference between the acoustic patterns associated to implant insertion with and without periprosthetic fractures was also evidenced by (31). Although the most common frequency of the acoustic signals was significantly different between the two situations, no quantitative information about the position nor the length of the fracture could be retrieve from these acoustic measurements. Eventually, another study (28) investigated the change of the bone-implant system vibration features due to periprosthetic fracture occurrence in an *in vivo* study. The correlation coefficient between the last two frequency response function (FRF) curves was used as a criterion to assess the implant insertion endpoint. During the experiments, it was shown that a lower value of the correlation coefficient was retrieved in the case of impending periprosthetic bone fracture. However, again, the change of the FRF was not analyzed in term of fracture properties.

Despite the identification of vibration or acoustic behavior changes following the fracture occurrence, the aforementioned studies did not propose a quantitative criterion for systematic periprosthetic fracture detection and assessment. The aim of the present study is to evaluate the sensitivity of a vibration method to detect periprosthetic fractures of different lengths, which are artificially created in bone mimicking phantoms. The employed technique is based on a previous work of our group (29) aiming at monitoring the FS insertion into the bone using a vibration measurement method applied to the blue inserter tool, called “ancillary” in what follows.

2 Materials and methods

2.1 Bone mimicking phantom specimens and FS implant

The study was performed on thirteen human artificial left femurs (ORTHObones, 3B Scientific, Hamburg, Germany). The bone mimicking phantoms were cut at the diaphysis level and the distal part was embedded in a fast-hardening resin (SmoothCast 300 polymer, Smooth-On, Easton, USA), similarly as in (29; 22), in order to be clamped to the fixed support. An uncemented FS implant of size 9, made of Ti-Al6-V4 titanium alloy and coated with hydroxyapatite was used throughout the study (CERAFIT R-MIS, Ceraver, Roissy, France). The host bone cavity was prepared by two experienced surgeons using the adapted rasps. The FS implant was fully inserted into the bone by successive hammer impacts on the ancillary, which is a square shape part made of stainless steel and temporary fixed to the FS during impaction. The insertion end-point was determined according to the surgeon proprioception. The vibration measurements were performed once the implant was fully inserted into the bone mimicking phantom.

2.2 Periprosthetic fracture creation

The periprosthetic fractures were artificially created in the 10 bone mimicking phantoms in order to control their initial position and plane of propagation and optimize the reproducibility as far as possible. Periprosthetic fractures located in the calcar zone, close to the lesser-trochanter, are considered throughout the study as they are the most frequent, with an occurrence rate reaching up to 42 % (12; 13). Such fractures correspond to type I as defined in (12), and to types A or B, depending on their length on the diaphysis femur region, according to the Vancouver classification (14; 18). The location and length of the fractures were both validated by an experienced orthopaedic surgeon.

A schematic description of the protocol used to reproduce fractures of different lengths is presented in Fig. 1. The periprosthetic fractures were initiated and enlarged once the implant was fully inserted into the bone mimicking phantom. The fracture was manually initiated in the trabecular bone at the bottom right corner of the bone cavity by a handsaw. Then, the fracture enlargement was achieved by impacting an osteotome in contact with the fracture line. Osteotomes are cutting tools usually used by orthopaedics and plastic surgeons to perform osteotomies (34). The fracture was iteratively enlarged as long as i) the fracture path stays on the part of the femur parallel to the plane (YZ) and ii) the fracture path length is lower than 40 mm. The length of the fracture was measured with a digital calliper after each enlargement. According to surgical observations, periprosthetic fracture lengths higher than 40 mm affect FS stability and are usually detected by the surgeon during the surgery (18). In what follows, for each specimen, i corresponds to the number of the fracture configuration, where $i \in \{1...n\}$, with n the number of the last fracture configuration. $i = 0$ corresponds to a non-fractured sample.

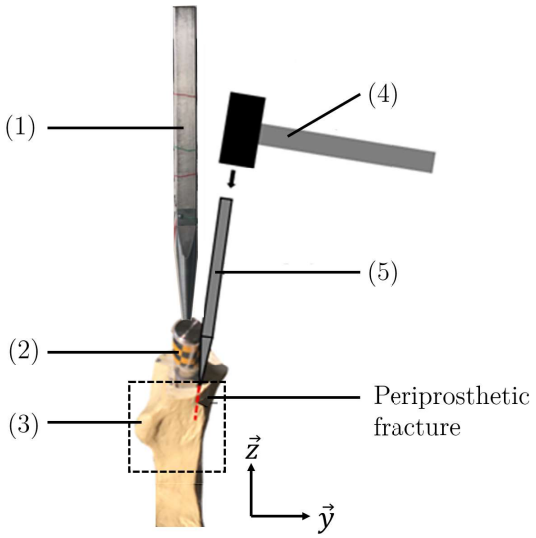

Figure 1: Schematic representation of the experimental set-up for periprosthetic fracture creation and enlargement. The dotted square indicates the calcar zone. (1) Ancillary, (2) FS implant, (3) Lesser-trochanter of the bone mimicking phantom, (4) Hammer and (5) Osteotome.

2.3 Resonance frequency measurements

2.3.1 Experimental set-up

Figure 2 shows a schematic description of the experimental set-up used to measure the resonance frequencies of the bone-stem-ancillary system. The bone mimicking phantom was clamped to the fixed support throughout the frequency measurements. The ancillary was equipped with two square piezoelectric sensors of 10 mm x 10 mm x 0.1 mm each (Plates, PI Ceramic, Lederhose, Germany) fixed on two perpendicular sides of the ancillary. The ancillary was screwed in the FS so that the normal of the piezoelectric sensor #1 (respectively #2) coincides with the y-direction (respectively x-direction) (see Fig. 2). Therefore, the piezoelectric sensor #1 (respectively #2) provides measurements of the resonance frequencies of the modes oscillating along y-direction (respectively x-direction). The positions of both piezoelectric sensors were determined in order to maximize the amplitude of the Frequency Response Functions (FRFs) at the resonances. These positions were chosen with regard to three bending modes identified in a previous experimental study of our group about the FS insertion monitoring (29): the modes $2Y$, $2Y_b$ and $2X$. The position of the sensor #1 (respectively #2) was optimized with regard to the mode shapes of the two modes $2Y$ and $2Y_b$ (respectively $2X$) oscillating along the y-direction (respectively x-direction) (29).

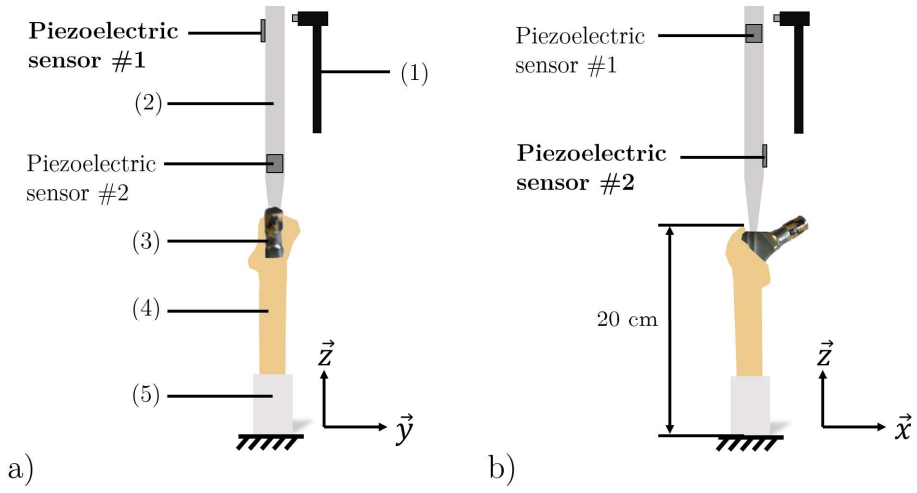

Figure 2: Experimental set up for FRF measurement of the bone-stem-ancillary's system with (a) the piezoelectric sensor #1 for an impact in y-direction and (b) the piezoelectric sensor #2 for an impact in x-direction. (1) Modal hammer, (2) Ancillary, (3) FS implant, (4) Bone mimicking phantom (5) Resin with clamping to the fixed support.

2.3.2 Measurement protocol

The measurement of the FRF of the ancillary was performed for each phantom and each fracture length, before the fracture was created and then, from the fracture initiation to a fracture length of at least 40 mm. The bone-stem-ancillary system was excited by a modal hammer (8204, Brüel and Kjaer, Naerum, Denmark), of 5g-mass, which enables frequency measurements within the range [0.4 - 12.8] kHz. The vibration response of the ancillary, measured by the piezoelectric sensors, was recorded by a dedicated data acquisition module (BK

Connect, Brüel and Kjaer, Naerum, Denmark) with a sampling rate of 51.2 kHz and a duration of 0.25 s. The frequency resolution was 1 Hz. The impacts were performed close to the top free extremity of the ancillary, in order to retrieve a maximum number of resonance frequencies on the FRF. Impacting close to a free extremity allows for being distant to a node of vibration which optimize resonance frequencies visibility on the FRF (35). The impacts were applied in both x- and y-directions, and the corresponding vibration signal was recorded by the piezoelectric sensor whose the normal is aligned with the direction of impact. Note that all measurements were repeated five times in each direction. The impacts were applied with a maximum force lower than 50 N in order to avoid any modification of the implant position, which could affect the FRF.

2.4 Data analysis of frequency measurements

2.4.1 Frequency response functions

The Frequency Response Functions (FRFs), noted h, were calculated in the frequency range $f \in [0.4-12.8]$ kHz as follows (35):

$$h(f) = \frac{\hat{p}(f)}{\hat{F}(f)} \tag{1}$$

where $\hat{p}$ and $\hat{F}$ denoted the Fourier Transforms (FTs) of the voltage and force signals, recorded by the piezoelectric sensor and the modal hammer, respectively.

2.4.2 Frequency sensitivity and minimal size of detectable fracture

The resonance frequency sensitivity to bone fracture detection for a given fracture configuration i was defined as the difference between the resonance frequency of the bone-stem-ancillary's system with a fracture in the configuration i (f_i) and without fracture for a complete insertion (f_0) and is given by:

$$\Delta f_{i/0} = f_i - f_0 \tag{2}$$

For each bone mimicking phantom specimen and each resonance frequency, $\Delta f_{i/0}$ was then analyzed as a function of the length l_i of the fracture at the configuration $\#i$.

A threshold for fracture detection, corresponding to the minimal frequency variation that could be detected using the measurement set-up, noted Δf_s, was defined for each resonance frequency f by:

$$\Delta f_s = \sigma_f + 1 \text{ Hz} \tag{3}$$

where 1 Hz corresponds to the data acquisition frequency resolution and σ_f is the standard deviation related to the measurement protocol obtained for each resonance frequency f. σ_f was evaluated by repeating the measurement protocol described in Section 2.3.2 fifteen times with the bone mimicking phantom #1, before any fracture was made, in both x- and y-directions. Therefore, fifteen FRFs were recorded by each piezoelectric sensor, and the standard deviation σ_f corresponding to each resonance frequency f was calculated.

A minimal detectable fracture's length, noted l_{min}, was then defined as the length corresponding to Δf_s, when plotting $\Delta f_{i/0}$ as a function of l_i for each resonance frequency f. However, as indicated in Section 2.2, the enlargement of the fracture was incremental and the measurements of the FRF were performed for discrete values of fracture lengths l. Therefore, a linear interpolation of the experimental data $\Delta f(l)$ was performed between the closest values surrounding Δf_s, in order to estimate l_{min}.

2.4.3 Statistical analysis

A one-way analysis of variance (ANOVA) and Tukey-Kramer tests were performed to evaluate the significance of minimal fracture length detection l_{min} as a function of the resonance frequency f. Statistical differences were defined at a 95 % confidence level.

3 Results

3.1 Fracture positions and lengths

An example of a bone fracture with typical enlargement steps $\#i$ is presented in Fig. 3 for the bone mimicking phantom #9. The fracture is initiated at the bottom right corner of the bone cavity ($i = 1$, Fig. 3a) and then it is successively enlarged from 8.74 mm ($i = 2$, Fig. 3b) to 54.9 mm ($n = 4$, Fig. 3d) following the protocol presented in Section 2.2. The final length of the fracture varies between 27.0 mm and 55.3 mm according to the bone mimicking phantom. For 3 out 10 specimens, the enlargement protocol was stopped because the fracture line direction went out of the (YZ) plane, which explains the small values of fracture lengths ($l < 40$ mm) obtained for these specimens at the last enlargement step n. Moreover, the fracture direction and length increments due to each enlargement step i are difficult to control because of the fragile behavior of the bone mimicking phantom material. The fracture path depends on multiple factors such as: the cutting tool angle, the impaction force, the exact geometry of the bone, the path direction changes between two specimens. Therefore, the number of steps to obtain a final fracture's length such as $l > 40$ mm varies between $n = 3$, 4 or 5 according to the specimen.

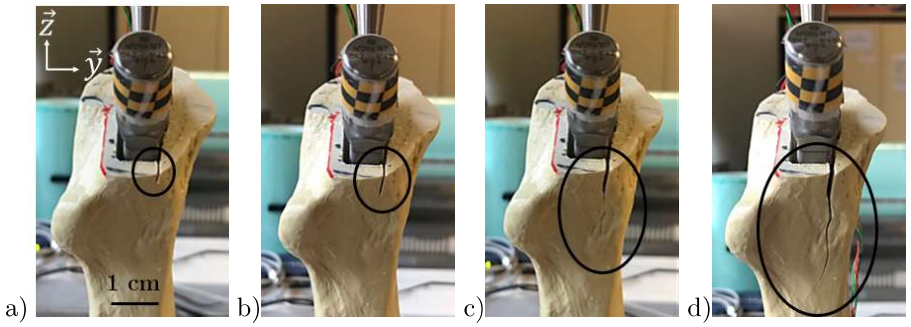

Figure 3: Pictures of typical fractures on bone mimicking phantom #9, from creation ($i = 0$) to final configuration ($i = n$). (a) $i = 1$, $l = 4.2$ mm, (b) $i = 2$, $l = 8.7$ mm, (c) $i = 3$, $l = 36.5$ mm and (d) $i = n$, $l = 54.9$ mm.

3.2 Choice of the resonance frequencies of interest

3.2.1 Frequency behavior without fracture

The resonance frequencies in the range [2-12] kHz of the bone-implant-ancillary system corresponding to a complete insertion in a non-fractured state are shown in Table 1 for the ten bone mimicking phantoms. The mean values of the modes as well as the standard deviation obtained over the specimens, corresponding to the inter-specimen variability are indicated. Four (respectively three) modes were identified in the plane (YZ) (respectively (XZ)) with the piezoelectric sensor #1 (respectively sensor #2) and were noted "Y_f" (respectively "X_f"), where "f" is the mean value f_{mean} (in kHz) of the resonance frequency of each mode obtained over the ten specimens (see Table 1). The modes are selected based on the results from a previous study on FS insertion monitoring (29). The modes "$Y_{2.6}$" and "$Y_{3.3}$", measured by the piezoelectric sensor #1 and the mode "$X_{3.2}$" measured by the piezoelectric sensor #2 correspond to the modes $2Y$, $2Y_b$ and $2X$, identified in (29), respectively. The modes $2Y$ and $2Y_b$ were shown to be highly sensitive to the implant insertion step (29). The four other modes were chosen for their good observability on the FRF, that is a peak amplitude at resonance frequency higher than 0.1 V/N and a small damping. The inter-specimen variability σ_{spec} for non-fractured specimen varies between 34 Hz and 194 Hz depending on the mode (see Table 1). This observation will be discussed in Section 4.1.1.

Specimen #	$\boldsymbol{Y_{2.6}}$	$\boldsymbol{Y_{3.3}}$	$\boldsymbol{Y_{4.2}}$	$\boldsymbol{Y_{11.1}}$	$\boldsymbol{X_{3.2}}$	$\boldsymbol{X_{6.4}}$	$\boldsymbol{X_{10.6}}$
1	2494	3060	3905	11094	3268	6383	10593
2	2696	3153	4110	11069	-	6412	10672
3	2572	3333	4129	10958	-	6415	10614
4	-	-	4205	11007	3237	6394	10640
5	2547	3329	4204	10833	3148	6323	10498
6	2627	3611	4321	11139	3263	6371	10629
7	2750	3489	4410	11124	3216	6409	10633
8	2644	3053	4342	11203	3320	6382	10561
9	2544	3460	4142	11046	3175	6351	10528
10	2586	3361	4081	11104	3209	6437	10666
$\boldsymbol{f_{mean}}$	2607	3317	4185	11058	3230	6388	10603
$\boldsymbol{\sigma_{spec}}$	81	194	147	105	55	34	58

Table 1: Values of the resonance frequency (in Hz) obtained for each mode and each bone specimen at the end of the insertion and before a fracture was created. The mean value f_{mean} over the ten specimens as well as the standard deviation σ_{spec} corresponding to the inter-specimen variability are indicated. The "-" symbol indicates that the mode could not be accurately measured for a given specimen and configuration.

An example of two FRFs of the bone-stem-ancillary system, noted h and measured by the piezoelectric sensors #1 (gray line) and #2 (black line) is shown in Figure 4 for the FS completely inserted into bone mimicking phantom #9 and before any fracture was initiated. The seven modes of interest are visible on the FRFs.

3.2.2 Method accuracy

Table 2 shows the standard deviation σ_f corresponding to each of the seven selected resonance frequencies f and calculated from the fifteen repeated measures of the frequency response functions h in the x- and y-directions

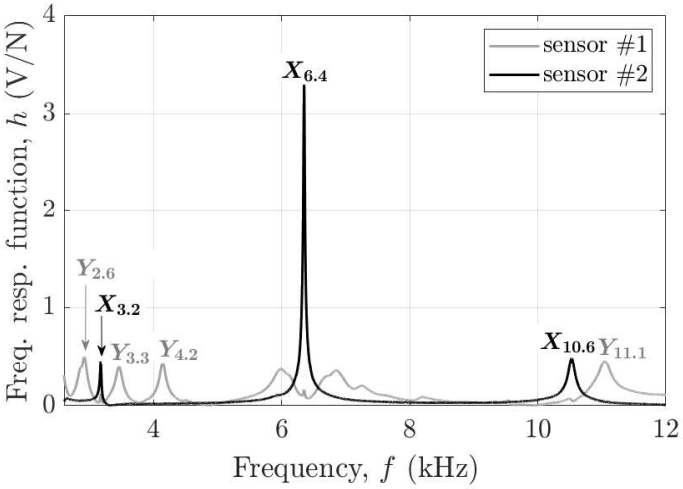

Figure 4: Frequency Response Functions (FRFs), h, of the bone-stem-ancillary's system, measured by the piezoelectric sensors #1 (gray line) and #2 (black line) for the bone mimicking phantom #9 before any fracture was created. The seven resonance frequencies f indicated on the curves are selected for the rest of the study. The mode $Y_{2.6}$ (respectively $Y_{3.3}$ and $X_{3.2}$) corresponds to the mode $2Y$ (respectively $2Y_b$ and $2X$) identified in (29).

by the piezoelectric sensors #2 and #1, respectively. The value of σ_f varies from 2 to 9 Hz according to the mode and is smaller for the resonance frequencies measured by the piezoelectric sensor #2.

Mode name	$\boldsymbol{Y_{2.6}}$	$\boldsymbol{Y_{3.3}}$	$\boldsymbol{Y_{4.2}}$	$\boldsymbol{Y_{11.1}}$	$\boldsymbol{X_{3.2}}$	$\boldsymbol{X_{6.4}}$	$\boldsymbol{X_{10.6}}$
σ_f (Hz)	4	3	9	3	2	2	2

Table 2: Standard deviation σ_f calculated for each resonance frequency of interest f from the fifteen frequency response functions h measured on a non-fractured bone mimicking phantom by the piezoelectric sensors #1 ($Y_{2.6}$, $Y_{3.3}$, $Y_{4.2}$ and $Y_{11.1}$) and the piezoelectric sensor #2 ($X_{3.2}$, $X_{6.4}$ and $X_{10.6}$).

3.3 Frequency sensitivity

3.3.1 Frequency shift quantification

Figure 5 shows the frequency response functions h of the bone-stem-ancillary system measured by the piezoelectric sensor #2 with a zoom on the three resonance frequencies of interest in the plane (XZ): the mode $X_{3.2}$ (a), the mode $X_{6.4}$ (b) and the mode $X_{10.6}$ (c). Each solid line corresponds to a different fracture enlargement state i, from $l = 4.24$ mm to $l = 54.9$ mm, created in the bone mimicking phantom specimen #9. The dashed lines correspond to the measurement of the non-fractured specimen ($i = 0$). The resonance frequencies of the three modes are decreasing functions of i, especially after the second enlargement of the fracture ($i > 1$), which corresponds to a fracture's length of $l = 8.74$ mm. The same results are obtained for the FRF measured by the piezoelectric sensor #1, with the modes $Y_{2.6}$, $Y_{3.3}$, $Y_{4.2}$ and $Y_{11.1}$ (data not shown).

The variation of the resonance frequency difference $\Delta f_{i/0}$ for bone mimicking phantom #9 as a function of l is shown in Fig. 6. The results are shown for the resonance frequencies measured by the piezoelectric sensor #1 (Fig. 6a) and by the piezoelectric sensor #2 (6b). For $i \geq 2$, $\Delta f_{i/0} > \sigma_f$ for each mode (see Table 2), which indicates that the resonance frequency variations can be used to detect bone fracture for a given specimen if the

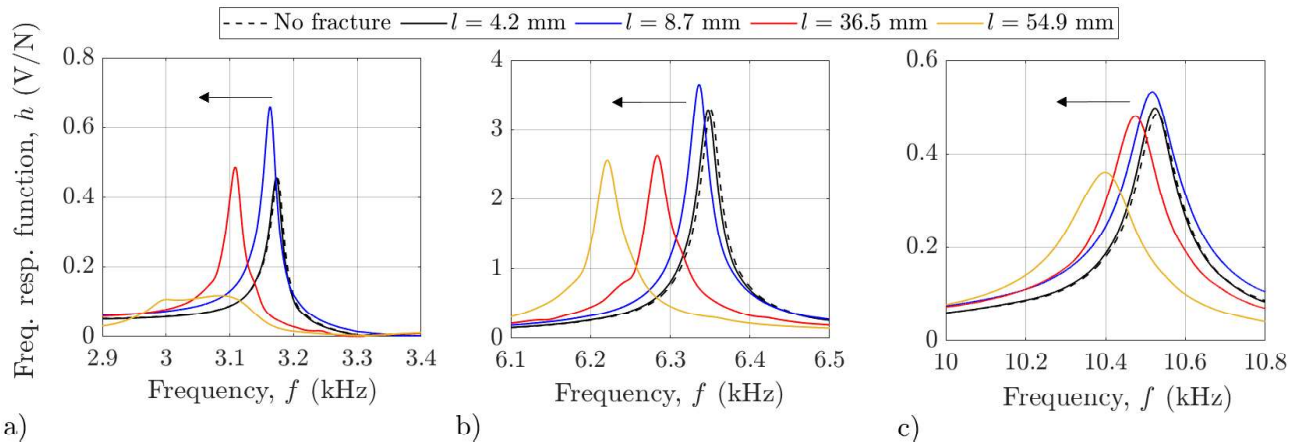

Figure 5: Zoom on the Frequency Response Function (FRF) h of the bone-stem-ancillary system around the resonance frequencies of interest corresponding to the modes $X_{3.2}$, $X_{6.4}$, $X_{10.6}$ measured by the piezoelectric sensor #2, for different fracture configurations i. The dashed and solid lines correspond to measurements for the non-fractured and fractured bone mimicking phantom specimen #9, respectively.

resonance frequency obtained in the non-fractured state is known. The value of $\Delta f_{4/0}$ obtained for the largest length $l = 54.9$ mm varies between 113 Hz and 170 Hz, according to the resonance frequency considered.

Figure 7 shows the results of the resonance frequency shifts of the mode $X_{10.6}$ as a function of the fracture length for the ten bone mimicking phantoms. Although the frequency shift increases as a function of the crack length, the data are quiet scattered because the fracture path, depth and thickness depend on the specimen, which could not be measured in this study.

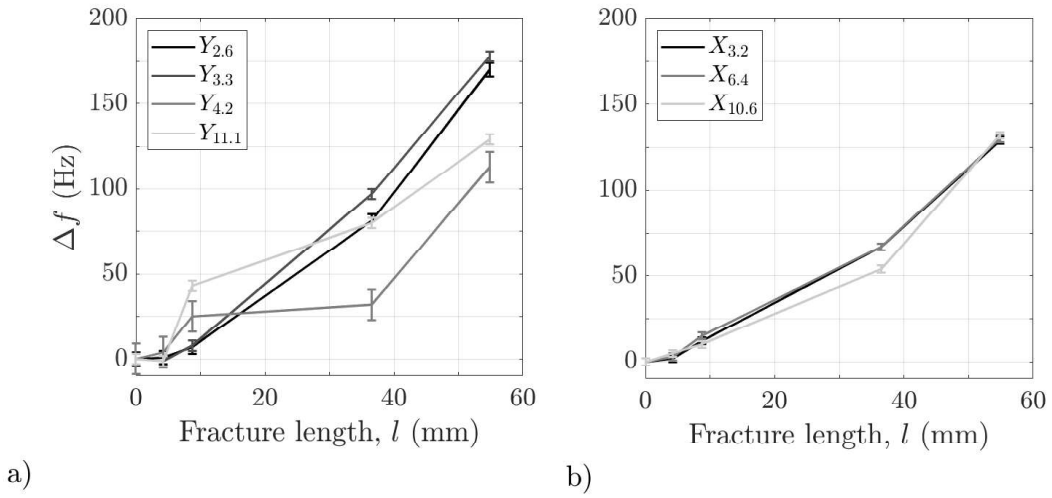

Figure 6: Variation of the resonance frequency difference $\Delta f_{i/0}$ measured for the bone mimicking phantom #9 between the fracture configuration i and the non-fractured specimen ($i = 0$) as a function of the fracture length l for both resonance frequencies measured by the piezoelectric sensor #1 (a) and #2 (b). The error bars correspond to the standard deviation σ_f calculated for each of the seven resonance frequency f.

3.3.2 Minimal fracture length detection

The values of the minimal fracture length l_{min} calculated from the threshold Δf_s defined by Eq. 3 and the results shown in Fig. 6 for the bone mimicking phantom #9 are l_{min} = 7.3 mm, 6.7 mm, 5.5 mm and 4.8 mm (respectively l_{min} = 4.7 mm, 4.2 mm and 2.5 mm) for the modes $Y_{2.6}$, $Y_{3.3}$, $Y_{4.2}$ and $Y_{11.1}$ measured

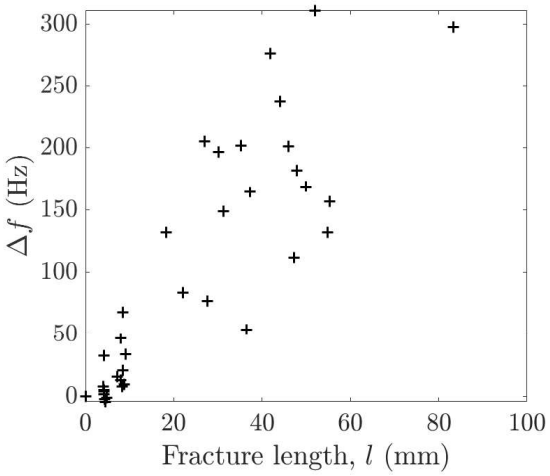

Figure 7: Frequency shifts of the mode $X_{10.6}$ as a function of the fracture length l obtained for the ten bone mimicking phantoms.

with piezoelectric sensor #1 (respectively for the modes $X_{3.2}$, $X_{6.4}$ and $X_{10.6}$ measured with piezoelectric sensor #2). Comparable results as the one shown in Fig. 6 were obtained for all bone mimicking phantoms (data not shown). The average values over all bone mimicking phantoms of the resonance frequency difference threshold Δf_s for fracture detection and the corresponding minimal fracture length l_{min}, associated to each resonance frequency f are shown in Table 3. The minimal fracture length l_{min} varies between 3.1 ± 1.7 mm and 5.9 ± 1.9 according to the resonance frequency f. ANOVA test of the results obtained with all ten bone mimicking phantoms was performed and the results show a significant effect of the mode on the minimal length of detectable fracture l_{min} (p-value = 0.011). Tukey-Kramer analysis indicates that the value of l_{min} obtained with the mode $X_{10.6}$ measured by piezoelectric sensor #2 is significantly lower from the results obtained with the mode $Y_{2.6}$ ($Y_{4.2}$ respectively) measured by piezoelectric sensor #1 (p-values = 0.016 and 0.013 respectively). However, the results obtained by the other modes are statistically similar and the mode $X_{10.6}$ appears to be the most sensitive to detect fracture occurring in the (YZ) plane.

Mode name	$\boldsymbol{Y_{2.6}}$	$\boldsymbol{Y_{3.3}}$	$\boldsymbol{Y_{4.2}}$	$\boldsymbol{Y_{11.1}}$	$\boldsymbol{X_{3.2}}$	$\boldsymbol{X_{6.4}}$	$\boldsymbol{X_{10.6}}$
Δf_s (Hz)	5	4	10	4	3	3	3
l_{min} (mm)	5.9 ± 1.9	5.4 ± 1.0	5.8 ± 1.5	4.4 ± 2.6	4.9 ± 1.0	5.0 ± 1.5	3.1 ± 1.7

Table 3: Resonance frequency difference thresholds for fracture detection, Δf_s, with the corresponding minimal length of detectable fracture, l_{min}, obtained for each resonance frequency f. The results are averaged over the ten bone mimicking phantom specimens.

4 Discussion

The main purpose of the present study was to investigate whether resonance frequency analysis can be used to detect periprosthetic fractures during FS implant insertion. The vibration analysis of the bone-stem-ancillary system had been previously studied by our group to monitor FS insertion (29). It had been shown that several resonance frequencies of the bone-stem-ancillary system in the range [2-6] kHz were sensitive to the implant insertion depth into the host bone. The originalities of the present work are i) to show that different resonance

frequencies are sensitive to the presence of periprosthetic fracture and ii) to provide a quantitative criterion for periprosthetic fracture detection, based on the bone-stem-ancillary's system resonance frequency shifts consecutive to the fracture creation and propagation. In particular, different sensitive resonance frequencies were identified and the minimal size of measurable periprosthetic fracture throughout resonance frequency analysis was evaluated for each vibration mode.

The frequency measurements were performed throughout the ancillary, considering different length of periprosthetic fractures which have been manually created. The frequency range was enlarged to [2-12] kHz compared to (29). The main advantage of performing measurements throughout the ancillary is that it does not require sensor fixation on the implant nor the bone, which allows to consider the use of such approach in clinical conditions in the future.

4.1 Detection of periprosthetic fractures by resonance frequency analysis

4.1.1 Bone-stem-ancillary vibration behavior

Seven resonance frequencies f could be identified in the frequency range [2-12] kHz for all ten bone mimicking phantom specimens and all states of periprosthetic fractures. Two directions of FRF measurements were analyzed thanks to two piezoelectric sensors fixed on two perpendicular faces of the ancillary. The positions of the piezoelectric sensors along the ancillary axis had been optimized in order to maximize the amplitude of the FRF at the resonances of the three modes identified in a previous study on FS insertion monitoring by means of modal analysis (29). In particular, the modes $Y_{2.6}$, $Y_{3.3}$ and $X_{3.2}$ analyzed in the present study correspond to the modes $2Y$, $2Y_b$ and $2X$ already identified in (29). The hypothesis was made that these modes, which are sensitive to the implant insertion depth could also be sensitive to periprosthetic fractures, which was confirmed in the present study (see Fig. 6a). For instance, the presence of a periprosthetic fracture of length $l = 54.9$ mm in the bone mimicking phantom #9 resulted in a decrease of the resonance frequency equal to 170 Hz (respectively 178 Hz and 129 Hz) for the mode $Y_{2.6}$ (respectively $Y_{3.3}$ and $X_{3.2}$) (see Fig. 6). Moreover, four supplementary modes with regard to the study of (29) were analyzed in the present work due to their high amplitude and small damping on the FRF (see Fig. 4): the modes $Y_{4.2}$ and $Y_{11.1}$ measured by the piezoelectric sensor #1 and the modes $X_{6.4}$ and $X_{10.6}$ measured by the sensor #2. In total, four (respectively three) resonance frequencies were analyzed in the present study from FRF measurements in the y-direction (respectively x-direction) using the piezoelectric sensor #1 (respectively #2) in the frequency range [2-12] kHz. The inter-specimen resonance frequency variability reaches up to 194 Hz for non-fractured specimen, depending on the mode (see Table 1). Note that the inter-specimen variability was investigated in a previous numerical study (36) and may be explained by slightly different implant positions at the end of insertion, different bone-implant macroscopic contact ratio or different bone stiffness over the specimens. In addition it was assumed that the bone-implant system behaves linearly during the modal tests, due to the low energy applied with the modal hammer (29). Eventually, we assumed that the weight of the piezoelectric sensors does not influence the frequency response of the bone-stem-ancillary system.

4.1.2 Resonance frequency sensitivity to periprosthetic fracture occurrence

For all the seven modes and the ten bone mimicking phantom specimens, a decrease of the resonance frequency values was obtained when the fracture length increased, as shown in Fig. 5 and 6 for bone mimicking phantom #9 and in Fig. 7 for all specimens and the mode $X_{10.6}$. The frequency shifts are of the same order of magnitude than the inter-specimen variability. However, the inter-specimen variability σ_{spec} does not affect the detection of the fracture by the method proposed herein, since the protocol consists in comparing at least two FRFs for a same specimen, one of which being for the non-fractured state. The decrease of pre-stressed state of the bone-implant system due to the fracture (19; 37) leads to a decrease of the system rigidity (18; 17; 4), which is responsible for a substantial change of the system vibro-acoustic response. In particular, the shift of the FRF to lower frequencies is consistent with a loss of rigidity of the system (24; 26; 38) due to the periprosthetic bone fracture. However, the change of press-fit due to the fracture should be high enough in order to be detected on the FRF's measurement. Figures 6 and 7 show that before a certain fracture length (l = 8.7 mm for the specimen #9), the resonance frequency variation compared to the non-fractured state is lower than the standard deviation of the measurement and thus the bone fracture cannot be detected. Although the frequency shift tends to increase as a function of the crack length, the data are quiet scattered because the fracture path, depth and thickness depend on the sample, which could not be measured in this study. It is worth noting that the periprosthetic fractures studied herein are among the less severe according to the Vancouver classification (17), with small consequences on the FS stability (18), which indicates the good sensitivity of the frequency method investigated in the present paper.

The decrease of the bone-stem-ancillary system resonance frequencies as a function of the fracture length is in agreement with previous numerical (39; 36) and *in vitro* (29) and *in vivo* (28) experimental studies. In (29), it was demonstrated that several resonance frequencies in the range [0.4-12.8] kHz increase during FS insertion depth into the host bone, which was associated to an increase of the global rigidity of the bone-stem-ancillary system. Moreover, the resonance frequency variation behavior with fracture occurrence agrees with observations made by (28) during *in vivo* measurements where the FRF's graphs were shifted to lower frequencies consecutively to fracture occurrence. The fracture was quantitatively noticed by lower values of correlation coefficient between the two last FRFs. The shift to lower frequencies is also coherent with numerical results (36), which showed that the resonance frequencies decreased when the trabecular bone Young's modulus decreased. Note that a bone damage like a fracture can be modeled by a local reduction of bone Young's modulus (40; 41). Eventually, the use of the mode shape curvature in order to detect the periprosthetic fractures, rather than the resonance frequency shift only, was also investigated (40). Curvature based-damage index are widely used in industrial engineering to localize and quantify structural damage (42; 43).

Acoustic methods, which have been investigated for acetabular cup (44) or FS insertion monitoring (33; 30; 32; 31) also showed that the resonance frequency was sensitive to periprosthetic fracture (13; 31; 30). In an *in vivo* study (30), the spectral analysis of the sound produced by the hammer impacts during implant insertion showed a drop of the band power features (BPF), which corresponds to the ratio of the power in a specific

frequency band over the total power of the frequency spectrum, with the occurrence of a micro or macro-fracture. Another clinical study (31) aiming at quantifying the sound produced during stem insertion found a significant relationship between the sound pattern and the occurrence of intra-operative fracture and subsidence. These two studies confirmed the sensitivity of the vibro-acoustic behavior of the bone-implant-ancillary's system to periprosthetic fracture occurrence, which is in agreement with the results found herein.

4.1.3 A quantitative criterion to detect periprosthetic fracture

The analysis of the FRF's measurements allowed the detection of periprosthetic fractures from 3.1 mm to 5.9 mm in length, depending on the resonance frequency (see Table 3). These sizes are relatively small compared to what the surgeons are able to detect during the surgery, making the method clinically relevant for early detection of periprosthetic bone fractures. In particular, the highest frequencies ($Y_{11.1}$ and $Y_{10.6}$) allowed the detection of the smallest fractures (see Table 3). This result emphasizes the role of higher resonance frequencies in local bone damage detection, whereas lower frequencies are sensitive to global change of rigidity of the bone-implant-ancillary system (28; 45; 30). Moreover, it was observed that the resonance frequency of the mode $X_{10.6}$ had a significantly higher sensitivity than the other resonance frequencies. This result can be explained by the direction of vibration of the mode $X_{10.6}$, which is purely normal to the fracture plane (YZ). This result indicates that sensor positioning should take into account the plane of the fracture that is to be detected.

4.2 Limitations and perspectives

The first limitation comes from the use of bone mimicking phantoms instead of human femurs. Only the proximal part of the femur was used, as it allows to fixed the specimen to a testing table (see Fig. 2). Although this configuration is commonly employed in the literature for numerical (39) or experimental studies (22; 29), the variation of boundary conditions, as well as changes in bone stiffness compared to the anatomic configuration may affect the resonance frequency values. Therefore, i) the same length of femur mimicking phantoms was considered for all the specimens and ii) the position and clamping of the specimen to the testing table were not changed throughout the experimental measurement. In addition, since the method consists in quantifying a frequency change with regard to the non-fractured bone for each specimen, the specific value of the resonance frequency has no relevance for the data analysis, except that it allows to identify the mode. Then, the presence of soft tissues surrounding the bone, as well as the use of a "wet" bone instead of bone mimicking phantom is expected to reduce the resonance frequencies values and to increase the damping (46) with regard to the results observed herein. The resistance to fracture of the femur is expected to be higher for a wet-bone than a bone mimicking phantom, since it increases with the bone quality (6; 47; 48). However, this difference of material property does not influence the results presented herein, since the fractures were manually created. In contrast, the absence of surrounding soft tissues could lead to an overestimation of the implant stability loss due to the fracture. Therefore, the presented results are likely to provide an overestimation of the frequency decrease, which could provide an earlier fracture detection than considering *in vivo* studies. The present *in vitro* study

should be considered as a demonstration of the feasibility to use resonance frequency analysis based method for periprosthetic fracture detection. The method developed in the present paper should be tested in anatomical subjects to retrieve quantitative frequency data, such as the bone-implant-ancillary resonance frequency functions and the identification of the frequency range of interest considering the anatomic configuration, which are necessary for the perspective of developing a future medical device that could be used in the clinic.

The second limitation lies in the difficulty to control and characterize the geometry of the fracture. First, the width of the fracture was not measured, as it is not constant along the fracture line. Then, the fracture depth across the cortical bone could not be retrieved whereas it may also influence the frequency sensitivity, especially for the bone around the FS. In addition, the length of the fracture was estimated with a numerical calliper and therefore, the total length of the fracture corresponds to the distance between the two extremities of the fracture line. However, the fracture path is not a straight line and this measure gives an insight of the approximate fracture length only. While this geometrical characterization may lead to errors due to the precision of the caliper (0.01 mm) and the manual measurement, it still gives a relevant order of magnitude of the minimal size of fracture which is detectable using resonance frequency analysis. Eventually, even if all periprosthetic fractures were initialized at the same point of the bone cavity and even if it was ensured that the fracture line stays in the plane (YZ) of the femoral bone mimicking phantom, the fracture line direction within the plane varies from one specimen to another, leading to different types of fractures among the specimens. The variability of the geometrical properties of the fracture may lead to slightly different FS stability loosening and thus different vibration behaviors, which may explained the values of the standard deviation σ_f associated to the minimal lengths of detectable fracture (see Table 3). In a future study, in addition to better characterize the geometrical properties of the fracture, it would also be relevant to investigate the sensitivity of the resonance frequency analysis to other types of fractures, and in particular fracture of types II described in (12). As these fractures occur in the plane (XZ), the resonance frequencies measured by the piezoelectric sensor whose the normal is perpendicular to this plane are expected to be more sensitive than resonance frequencies measured in the other perpendicular plane.

The third limitation concerns the method used for the estimation of the minimal detectable fracture length l_{min}. It was chosen to define l_{min} as the fracture length corresponding to the resonance frequency sensitivity threshold Δf_s. Therefore, a linear extrapolation between the two experimental points closest to Δf_s was performed in order to calculate l_{min}. However, this approximation can lead to an overestimation of the method performance to detect small fractures, as it is not known whether the resonance frequency sensitivity Δf increases linearly as a function of the fracture length l, between the two experimental points around Δf_s. Therefore, additional fracture enlargement states i should be considered, especially for the small fractures, which would increase the accuracy of the estimation of l_{min}. Here, the estimation was performed on a fracture length increment of the order of 5 mm in the present study.

Eventually, a fourth limitation consists in the fact that the fracture was manually created, while it would be of interest that the method proposed herein could detect a fracture occurrence during the implant insertion. Therefore, based on the preliminary results obtained in the present study, a future objective will be to move

towards a real-time method, capable of either preventing or detecting bone fracture occurrence throughout the implant insertion using hammer impacts.

5 Conclusions

The present paper investigates the use of a vibration-based method for the intra-operative detection of periprosthetic femoral bone fractures. This study is the first *in vitro* validation and quantification of the sensitivity of the bone-stem-ancillary system resonance frequencies to periprosthetic fracture occurrence of different lengths. A periprosthetic fracture was artificially created and enlarged in ten bone mimicking phantom in the calcar zone, close to the lesser-trochanter. A resonance frequency shift to lower frequencies due to the fracture occurrence and propagation was observed and quantified for seven resonance frequencies in the range [2–12] kHz. A frequency sensitivity threshold was defined and the corresponding minimal length of noticeable fracture was calculated for each resonance frequency. A statistical analysis reveals a significantly higher sensitivity for one of the highest resonance frequencies, corresponding to a bending mode vibrating in a plane perpendicular to the fracture path. The method should be tested on anatomical subjects to be closer to real clinical conditions, with the future perspective of developing a medical device for intra-operative periprosthetic fracture detection.

6 Acknowledgments

The authors would like to thank Oriane Le Demeet for help in obtaining experimental results.

7 Funding

This project has received funding from the European Research Council (ERC) under the European Union's Horizon 2020 research and innovation program (grant agreement No 682001, project ERC Consolidator Grant 2015 BoneImplant), from the project OrthAncil (ANR-21-CE19-0035-03) and from the project OrthoMat (ANR-21-CE17-0004).

8 Declaration of Conflicting Interests

The authors declare that they have no financial or non-financial interests that are directly or indirectly related to the work submitted for publication.

References

[1] Singh JA, Yu S, Chen L, Cleveland JD. Rates of Total Joint Replacement in the United States: Future Projections to 2020–2040 Using the National Inpatient Sample. Journal of Rheumatology. 2019 Sep;46(9):1134-40.

[2] Troelsen A, Malchau E, Sillesen N, Malchau H. A review of current fixation use and registry outcomes in total hip arthroplasty: the uncemented paradox. Clinical Orthopaedics and Related Research®. 2013 Jul;471(7):2052-9.

[3] Fitzgerald RHJ, Brindley GW, Kavanagh BF. The Uncemented Total Hip Arthroplasty: Intraoperative Femoral Fractures. Clinical Orthopaedics and Related Research®. 1988 Oct;235:61-6.

[4] Schwartz JT, Mayer JG, Engh CA. Femoral fracture during non-cemented total hip arthroplasty. Journal of Bone and Joint Surgery American Volume. 1989 Sep;71(8):1135-42.

[5] Abdel MP, Watts CD, Houdek MT, Lewallen DG, Berry DJ. Epidemiology of periprosthetic fracture of the femur in 32 644 primary total hip arthroplasties: a 40-year experience. The Bone & Joint Journal. 2016 Apr;98-B(4):461-7.

[6] Sidler-Maier CC, Waddell JP. Incidence and predisposing factors of periprosthetic proximal femoral fractures: a literature review. International Orthopaedics. 2015 Sep;39(9):1673-82.

[7] Berry DJ. Epidemiology: Hip and Knee. Orthopedic Clinics of North America. 1999 Apr;30(2):183-90.

[8] Meek RMD, Garbuz DS, Masri BA, Greidanus NV, Duncan CP. Intraoperative fracture of the femur in revision total hip arthroplasty with a diaphyseal fitting stem. Journal of Bone and Joint Surgery American Volume. 2004 Mar;86(3):480-5.

[9] Berend ME, Smith A, Meding JB, Ritter MA, Lynch T, Davis K. Long-term outcome and risk factors of proximal femoral fracture in uncemented and cemented total hip arthroplasty in 2551 hips. Journal of Arthroplasty. 2006 Sep;21(6 Suppl 2):53-9.

[10] Miettinen SSA, Mäkinen TJ, Kostensalo I, Mäkelä K, Huhtala H, Kettunen JS, et al. Risk factors for intraoperative calcar fracture in cementless total hip arthroplasty. Acta Orthopaedica. 2016;87(2):113-9.

[11] Lamb JN, Matharu GS, Redmond A, Judge A, West RM, Pandit HG. Risk Factors for Intraoperative Periprosthetic Femoral Fractures During Primary Total Hip Arthroplasty. An Analysis From the National Joint Registry for England and Wales and the Isle of Man. Journal of Arthroplasty. 2019 Dec;34(12):3065-73.

[12] Ferbert T, Jaber A, Gress N, Schmidmaier G, Gotterbarm T, Merle C. Impact of intraoperative femoral fractures in primary hip arthroplasty: a comparative study with a mid-term follow-up. Hip International: The Journal of Clinical and Experimental Research on Hip Pathology and Therapy. 2020 Sep;30(5):544-51.

[13] Sakai R, Kikuchi A, Morita T, Takahira N, Uchiyama K, Yamamoto T, et al. Hammering sound frequency analysis and prevention of intraoperative periprosthetic fractures during total hip arthroplasty. Hip International: The Journal of Clinical and Experimental Research on Hip Pathology and Therapy. 2011 Dec;21(6):718-23.

[14] Duncan CP, Masri BA. Fractures of the femur after hip replacement. Instructional course lectures. 1995 Jan;44:293-304.

[15] Brady OH, Garbuz DS, Masri BA, Duncan CP. The reliability of validity of the Vancouver classification of femoral fractures after hip replacement. Journal of Arthroplasty. 2000 Jan;15(1):59-62.

[16] Rayan F, Dodd M, Haddad FS. European validation of the Vancouver classification of periprosthetic proximal femoral fractures. Journal of Bone and Joint Surgery British volume. 2008 Dec;90-B(12):1576-9.

[17] Mondanelli N, Troiano E, Facchini A, Ghezzi R, Di Meglio M, Nuvoli N, et al. Treatment Algorithm of Periprosthetic Femoral Fracturens. Geriatric Orthopaedic Surgery & Rehabilitation. 2022;13:21514593221097608.

[18] Masri BA, Meek RMD, Duncan CP. Periprosthetic Fractures Evaluation and Treatment. Clinical Orthopaedics and Related Research®. 2004 Mar;420:80-95.

[19] Fishkin Z, Han SM, Ziv I. Cerclage wiring technique after proximal femoral fracture in total hip arthroplasty. Journal of Arthroplasty. 1999 Jan;14(1):98-101.

[20] Berend KR, Lombardi AV, Mallory TH, Chonko DJ, Dodds KL, Adams JB. Cerclage wires or cables for the management of intraoperative fracture associated with a cementless, tapered femoral prosthesis: Results at 2 to 16 Years. Journal of Arthroplasty. 2004 Oct;19(7, Supplement 2):17-21.

[21] Ponzio DY, Shahi A, Park AG, Purtill JJ. Intraoperative Proximal Femoral Fracture in Primary Cementless Total Hip Arthroplasty. Journal of Arthroplasty. 2015 Aug;30(8):1418-22.

[22] Tijou A, Rosi G, Vayron R, Lomami HA, Hernigou P, Flouzat-Lachaniette CH, et al. Monitoring cementless femoral stem insertion by impact analyses: An in vitro study. Journal of the Mechanical Behavior of Biomedical Materials. 2018 Dec;88:102-8.

[23] Dubory A, Rosi G, Tijou A, Lomami HA, Flouzat-Lachaniette CH, Haïat G. A cadaveric validation of a method based on impact analysis to monitor the femoral stem insertion. Journal of the Mechanical Behavior of Biomedical Materials. 2019 Nov;103:103535.

[24] Albini Lomami H, Damour C, Rosi G, Poudrel AS, Dubory A, Flouzat-Lachaniette CH, et al. Ex vivo estimation of cementless femoral stem stability using an instrumented hammer. Clinical Biomechanics. 2020 Jun;76:105006.

[25] Lannocca M, Varini E, Cappello A, Cristofolini L, Bialoblocka E. Intra-operative evaluation of cementless hip implant stability: A prototype device based on vibration analysis. Medical Engineering & Physics. 2007 Oct;29(8):886-94.

[26] Oberst S, Baetz J, Campbell G, Lampe F, Lai JCS, Hoffmann N, et al. Vibro-acoustic and nonlinear analysis of cadavric femoral bone impaction in cavity preparations. MATEC Web of Conferences. 2018;148:14007.

[27] Kikuchi S, Mikami K, Nakashima D, Kitamura T, Hasegawa N, Nishikino M, et al. Laser Resonance Frequency Analysis: A Novel Measurement Approach to Evaluate Acetabular Cup Stability During Surgery. Sensors. 2019 Nov;19(22).

[28] Pastrav LC, Jaecques SV, Jonkers I, Perre GVd, Mulier M. In vivo evaluation of a vibration analysis technique for the per-operative monitoring of the fixation of hip prostheses. Journal of Orthopaedic Surgery and Research. 2009 Apr;4:10.

[29] Poudrel AS, Rosi G, Nguyen VH, Haiat G. Modal Analysis of the Ancillary During Femoral Stem Insertion: A Study on Bone Mimicking Phantoms. Annals of Biomedical Engineering. 2022 Jan;50(1):16-28.

[30] Goossens Q, Pastrav L, Roosen J, Mulier M, Desmet W, Vander Sloten J, et al. Acoustic Analysis to Monitor Implant Seating and Early Detect Fractures in Cementless Tha: An in Vivo Study. Journal of Orthopaedic Research: Official Publication of the Orthopaedic Research Society. 2020 Aug.

[31] Morohashi I, Iwase H, Kanda A, Sato T, Homma Y, Mogami A, et al. Acoustic pattern evaluation during cementless hip arthroplasty surgery may be a new method for predicting complications. SICOT-J. 2017;3.

[32] Wei J, Crezee W, Jongeneel H, Haas T, Kool W, Blaauw B, et al. Using Acoustic Vibrations as a Method for Implant Insertion Assessment in Total Hip Arthroplasty. Sensors. 2022 Feb;22:1609.

[33] Whitwell G, Brockett CL, Young S, Stone M, Stewart TD. Spectral analysis of the sound produced during femoral broaching and implant insertion in uncemented total hip arthroplasty. Proceedings of the Institution of Mechanical Engineers Part H, Journal of Engineering in Medicine. 2013 Feb;227(2):175-80.

[34] Lamassoure L, Giunta J, Rosi G, Poudrel AS, Meningaud JP, Bosc R, et al. Anatomical subject validation of an instrumented hammer using machine learning for the classification of osteotomy fracture in rhinoplasty. Medical Engineering & Physics. 2021 Sep;95:111-6.

[35] Ewins DJ. Modal testing: theory, practice, and application. 2nd ed. No. 10 in Mechanical engineering research studies. Baldock, Hertfordshire, England ; Philadelphia, PA: Research Studies Press; 2000.

[36] Poudrel AS, Nguyen VH, Rosi G, Haiat G. Influence of the biomechanical environment on the femoral stem insertion and vibrational behavior: a 3-D finite element study. Biomechanics and Modeling in Mechanobiology. 2022 Dec.

[37] Bishop NE, Höhn JC, Rothstock S, Damm NB, Morlock MM. The influence of bone damage on press-fit mechanics. Journal of Biomechanics. 2014 Apr;47(6):1472-8.

[38] Henyš P, Čapek L. Impact Force, Polar Gap and Modal Parameters Predict Acetabular Cup Fixation: A Study on a Composite Bone. Annals of Biomedical Engineering. 2018 Apr;46(4):590-604.

[39] Pérez MA, Seral-García B. A finite element analysis of the vibration behaviour of a cementless hip system. Computer Methods in Biomechanics and Biomedical Engineering. 2013;16(9):1022-31.

[40] Henyš P, Leuridan S, Goossens Q, Mulier M, Pastrav L, Desmet W, et al. Modal frequency and shape curvature as a measure of implant fixation: A computer study on the acetabular cup. Medical Engineering & Physics. 2018 Oct;60:30-8.

[41] Ovesy M, Aeschlimann M, Zysset PK. Explicit finite element analysis can predict the mechanical response of conical implant press-fit in homogenized trabecular bone. Journal of Biomechanics. 2020 Jun;107:109844.

[42] Pandey AK, Biswas M, Samman MM. Damage detection from changes in curvature mode shapes. Journal of Sound and Vibration. 1991 Mar;145(2):321-32.

[43] Abdel wahab MM, De roeck G. Damage detection in bridges using modal curvatures: application to a real damage scenario. Journal of Sound and Vibration. 1999 Sep;226(2):217-35.

[44] Goossens Q, Leuridan S, Henyš P, Roosen J, Pastrav L, Mulier M, et al. Development of an acoustic measurement protocol to monitor acetabular implant fixation in cementless total hip Arthroplasty: A preliminary study. Medical Engineering & Physics. 2017 Nov;49:28-38.

[45] Henys P, Capek L, Fencl J, Prochazka E. Evaluation of acetabular cup initial fixation by using resonance frequency principle. Proceedings of the Institution of Mechanical Engineers, Part H: Journal of Engineering in Medicine. 2015 Jan;229(1):3-8.

[46] Athanassoulis Makris G, Pastrav L, Goossens Q, Timmermans M, Mulier M, Vles G, et al. Influence of Artificial Soft Tissue on Intra-Operative Vibration Analysis Method for Primary Fixation Monitoring in Cementless Total Hip Arthroplasty. Applied Sciences. 2022 Apr;12:4027.

[47] Leuridan S, Goossens Q, Pastrav L, Roosen J, Mulier M, Denis K, et al. Determination of replicate composite bone material properties using modal analysis. Journal of the Mechanical Behavior of Biomedical Materials. 2017;66:12-8.

[48] Lamassoure L, Giunta J, Rosi G, Poudrel AS, Bosc R, Haiat G. Using an Impact Hammer to Perform Biomechanical Measurements during Osteotomies: Study of an Animal Model. Proceedings of the Institution of Mechanical Engineers Part H, Journal of engineering in medicine. 2021 Apr;235:9544119211011824.